



# Unraveling reaction discrepancy and electrolyte stabilizing effects of auto-oxygenated porphyrin catalysts in lithium–oxygen and lithium–air cells

Boran Kim<sup>1</sup> | Hyunyoung Park<sup>2,3</sup> | Hyun-Soo Kim<sup>1</sup> | Jun Seo Lee<sup>1</sup> | Jongsoon Kim<sup>2,3</sup>  | Won-Hee Ryu<sup>1</sup> 

<sup>1</sup>Department of Chemical and Biological Engineering, Sookmyung Women's University, Yongsan-gu, Seoul, Republic of Korea

<sup>2</sup>Department of Energy Science, Sungkyunkwan University, Jangan-gu, Suwon, Republic of Korea

<sup>3</sup>SKKU Institute of Energy Science and Technology (SIEST), Sungkyunkwan University, Jangan-gu, Suwon, Republic of Korea

## Correspondence

Jongsoon Kim, Department of Energy Science, Sungkyunkwan University, 2066 Seobu-ro, Jangan-gu, Suwon 16419, Republic of Korea.

Email: [jongsoonkim@skku.edu](mailto:jongsoonkim@skku.edu)

Won-Hee Ryu, Department of Chemical and Biological Engineering, Sookmyung Women's University, 100 Cheongpa-ro 47-gil, Yongsan-gu, Seoul 04310, Republic of Korea.

Email: [whryu@sookmyung.ac.kr](mailto:whryu@sookmyung.ac.kr)

## Funding information

National Research Foundation of Korea, Grant/Award Numbers:

2022M3J1A1085410, RS-2023-00208983

## Abstract

Lithium–oxygen (Li–O<sub>2</sub>) batteries are an emerging energy storage alternative with the potential to meet the recent increase in demand for high-energy-density batteries. From a practical viewpoint, lithium–air (Li–Air) batteries using ambient air instead of pure oxygen could be the final goal. However, the slow oxygen reduction and evolution reactions interfere with reversible cell operation during cycling. Therefore, research continues to explore various catalyst materials. The present study attempts to improve the performance of Li–Air batteries by using porphyrin-based materials known to have catalytic effects in Li–O<sub>2</sub> batteries. The results confirm that the iron phthalocyanine (FePc) catalyst not only exhibits a catalytic effect in an air atmosphere with a low oxygen fraction but also suppresses electrolyte decomposition by stabilizing superoxide radical ions (O<sub>2</sub><sup>•−</sup>) at a high voltage range. Density functional theory calculations are used to gain insight into the exact FePc-mediated catalytic mechanism in Li–Air batteries, and various ex situ and in situ analyses reveal the reversible reactions and structural changes in FePc during electrochemical reaction. This study provides a practical solution to ultimately realize an air-breathing battery using nature-friendly catalyst materials.

## KEYWORDS

catalyst, lithium–air battery, lithium–oxygen battery, phthalocyanine, redox mediator

## 1 | INTRODUCTION

Lithium–oxygen (Li–O<sub>2</sub>) batteries (LOBs) are known as one of the most promising energy storage systems due to their exceptional theoretical energy density (over 3500 Wh kg<sup>−1</sup>),

obtained using lightweight elements such as Li and O.<sup>1–4</sup> At the cathode, the oxygen reduction reaction (ORR) occurs during the discharge process, converting gaseous O<sub>2</sub> into solid Li<sub>x</sub>O<sub>2</sub> (x = 1 or 2) by reacting with Li<sup>+</sup> ions to form solid-state Li<sub>x</sub>O<sub>2</sub> products. Then, the discharge products

Boran Kim and Hyunyoung Park contributed equally to this study.

This is an open access article under the terms of the [Creative Commons Attribution](https://creativecommons.org/licenses/by/4.0/) License, which permits use, distribution and reproduction in any medium, provided the original work is properly cited.

© 2024 The Authors. *Carbon Energy* published by Wenzhou University and John Wiley & Sons Australia, Ltd.

reversibly decompose during the recharge process called oxygen evolution reaction (OER) ( $x\text{Li}^+ + \text{O}_2 + xe^- \leftrightarrow \text{Li}_x\text{O}_2$ ,  $x = 1$  or  $2$ ).<sup>5,6</sup> However, the inherent insulating properties of the discharge products negatively influence the OER kinetics and efficiency during the charging process, thereby causing high overpotential and low cycle performance in LOBs.<sup>7,8</sup>

To solve this problem, various attempts have been made to facilitate the oxidation of intrinsic  $\text{Li}_x\text{O}_2$  upon charging by exploring solid-state catalysts for LOBs.<sup>9-15</sup> While these catalysts successfully facilitate the  $\text{Li}-\text{O}_2$  reaction, they are easily deactivated by the formation of  $\text{Li}_x\text{O}_2$  products on the electrode surface, which causes unexpected decomposition in the electrolyte solvent and discharge products. Limited solid–solid contact between the solid catalyst and discharge products is also considered a hindrance in effectively catalyzing the reaction of LOBs. To address this issue, a category of soluble catalysts called redox mediators (RMs) have been introduced to remedy the shortcomings of solid-state catalysts. The RM catalyst directly dissolves in the electrolyte, enabling sufficient liquid–solid contact and inhibiting its deactivation by the formation of discharge products on the surface. The RM participates in the electrochemical reaction through direct oxidation and reduction during the discharge and charge processes. RMs are directly reduced and oxidized ( $\text{RM} + e^- \rightarrow \text{RM}^{\text{red}}$ ,  $\text{RM} \rightarrow \text{RM}^{\text{ox}} + e^-$ ) with lower overpotential instead of the formation and decomposition of discharge product as slow electrochemical reaction pathway during discharge or charge, respectively.<sup>16</sup> After the alternative reaction, the reduced or oxidized RMs help chemically to form or decompose the discharge product, respectively. For example, metal phthalocyanine (MPC)-based RMs exhibit exceptional catalytic activities and  $\text{O}_2$  binding properties on their porphyrin ring structures, thereby achieving reduced overpotential and improved energy efficiency in LOBs.

To practically advance existing LOB technology, proper operation of ambient air-breathing batteries should be guaranteed without the use of pure  $\text{O}_2$  gas. However, it is necessary to solve the practical limitations of using RM as an electrolyte catalyst for LOB in atmospheric air that contains low  $\text{O}_2$  concentrations ( $< 20\%$ ) and minor foreign gases (e.g.,  $\text{CO}_2$ ). These minor gases would react with the active components in the battery, resulting in unstable cyclability due to the generation of by-products. Therefore, the optimal RM catalyst for LOBs in real air atmosphere should (i) diffuse easily in the electrolyte to rapidly transfer electrons to the electrode, (ii) bind spontaneously with  $\text{O}_2$ , and (iii) transport the  $\text{O}_2$  efficiently to the cathode even at low  $\text{O}_2$  concentrations in a real air atmosphere with irreversible side reactions with minor foreign

gases.<sup>17-21</sup> Nevertheless, the detailed mechanism regarding the reaction characteristics of lithium–air (Li–Air)-breathing batteries (LABs) employing oxygenated RMs (e.g., MPC) in air atmosphere has not been sufficiently studied.

In this study, we unravel the intrinsic reaction characteristics of iron phthalocyanine (FePC) as an electrolyte catalyst in different atmospheric environments using  $\text{O}_2$  and air-breathing cells (Figure 1). FePC is an aromatic macrocyclic organic compound with the molecular formula of  $(\text{C}_8\text{H}_4\text{N}_2)_4\text{Fe}$ . It has been studied as a promising bifunctional electrocatalyst in LOBs due to its tunable catalytic activity, versatile functionality, natural abundance, and so on.<sup>21-27</sup>

Herein, we demonstrate the unique electrochemical behavior and catalytic effect of FePC on  $\text{O}_2$  and  $\text{CO}_2$  molecules in LABs using first-principles calculations and various experiments. In particular, the experimental results of the rotating ring disk electrode (RRDE) technique clearly showed the detailed reaction mechanism and electrolyte-stabilizing properties of FePC and its outstanding RM catalytic activity in both LOBs and LABs. The enhanced reversibility of LABs employing FePC is also confirmed via a number of ex situ characterization techniques. In addition, the reversible gas evolution reactions in FePC-containing LOBs and LABs during the charging process are successfully revealed through in situ differential electrochemical mass spectrometry (DEMS) analyses. Our study provides practical insights toward ultimately realizing the air-breathing battery and contributes to the development of auto-oxygenated organometallic soluble catalysts for environmentally friendly and cost-effective air-breathing battery technology.

## 2 | LI- $\text{O}_2$ /LI-AIR CELL REACTION CATALYZED BY AN FEPC

### 2.1 | Electrochemical properties of Li- $\text{O}_2$ /Li-Air cell, catalyzed by an FePC

We investigated the electrochemical properties of an FePC-containing LAB to verify the catalytic efficiency of FePC. As shown in Figure 2A, cyclic voltammetry (CV) results for pristine and FePC-containing LABs are compared to confirm the redox properties of FePC during charge/discharge. In FePC-containing LABs, the redox peaks appear around 2.3 V in the cathodic region. These peaks correspond to the Li–Air reaction originating from  $\text{O}_2$  species bound in FePC. The FePC-containing LAB exhibits a higher current compared with the pristine LAB, implying that FePC delivers better catalytic

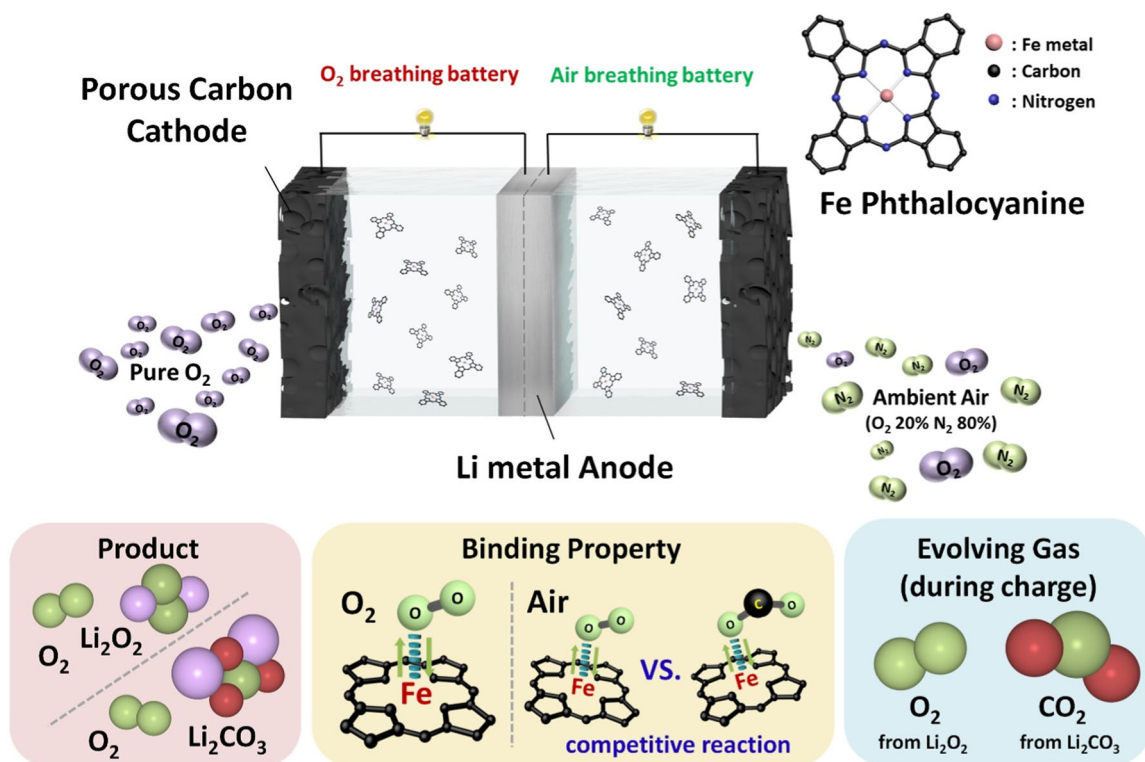


**FIGURE 1** Schematic illustration of the representative properties of FePc and an illustration showing the research concept using FePc as a redox mediator in  $O_2$  and air atmospheres.

performance during discharge/charge, even in low  $O_2$  atmospheres. Moreover, the potential difference between the onset potentials of the ORR (2.9 V) and OER (3.2 V) in the FePc-containing LAB was only 0.3 V, which is smaller than that in the pristine LAB (0.73 V). This demonstrates the enhancement in cell reversibility induced by the FePc catalyst for both the charge and discharge reactions. Other redox peaks are observed at 4.1 V in the anodic region and are associated with the  $Fe^{2+/3+}$  redox reaction.<sup>28,29</sup> In Figure 2B, the pristine LAB shows a lower discharge plateau around 2.65 V, whereas the FePc-containing LAB delivers an improved discharge overpotential ( $\sim 2.7$  V). In addition, FePc exhibits a catalytic activity in the charge process. The inclusion of FePc significantly reduces the OER overpotential compared with that of the cell without FePc. This can be interpreted by the faster  $O_2$  transfer achieved using FePc as an RM even in air, which results in a relatively lower overpotential. The difference is visible more clearly in the individual charge/discharge profiles collected at various cycles with a capacity limit of  $1000 \text{ mAh g}^{-1}$  (Figure 2C,D). In the pristine LAB without FePc, the overpotential ( $\sim 1.25$  V) is high during the initial cycle but becomes unstable after the 10th cycle. By contrast, the FePc-containing LAB shows a relatively reduced overpotential ( $\sim 0.85$  V) with stable cycle performance.

The results of the electrochemical experiments confirm the catalytic effect of FePc even in an air atmosphere with a low  $O_2$  concentration. However, since ambient air contains not only pure oxygen but also nitrogen and trace amounts of carbon dioxide ( $CO_2$ ), the electrochemical reaction of  $CO_2$  should also be taken into consideration. To elucidate the redox reaction mechanism of FePc in air, we coupled RRDE with chronoamperometry (Figure 2E). RRDE allows the quantification of the amount of soluble intermediates released during oxidation in real time.<sup>30</sup> The glassy carbon (GC) disk electrodes were first held at a cathodic voltage of 2.0 V versus  $Li^+/Li$  ( $V_{Li}$ ) to form the discharge products on the disk electrode surface to a consistent capacity of 0.4 mC. After discharge, reverse chronoamperometry was carried out to investigate the oxidation behavior of the discharge products ( $Li_xO_2$ ,  $Li_2CO_3$ ) on the disk and the subsequent oxidation of soluble  $LiO_2$  on the ring.<sup>30,31</sup> The  $LiO_2$  forming from the residual oxide intermediate after  $Li_2O_2$  oxidation diffuses from the disk to the ring by convective flow (Figure 2E). The  $Li_xO_2$  and  $Li_2CO_3$  on the disk decompose into their soluble forms during the charge reaction and move from the disk to the ring via rotational flow. We applied various charging voltages (3.3–4.2 V) to the disk and a constant charge voltage of 4.2 V on the ring. We considered that a charge voltage of

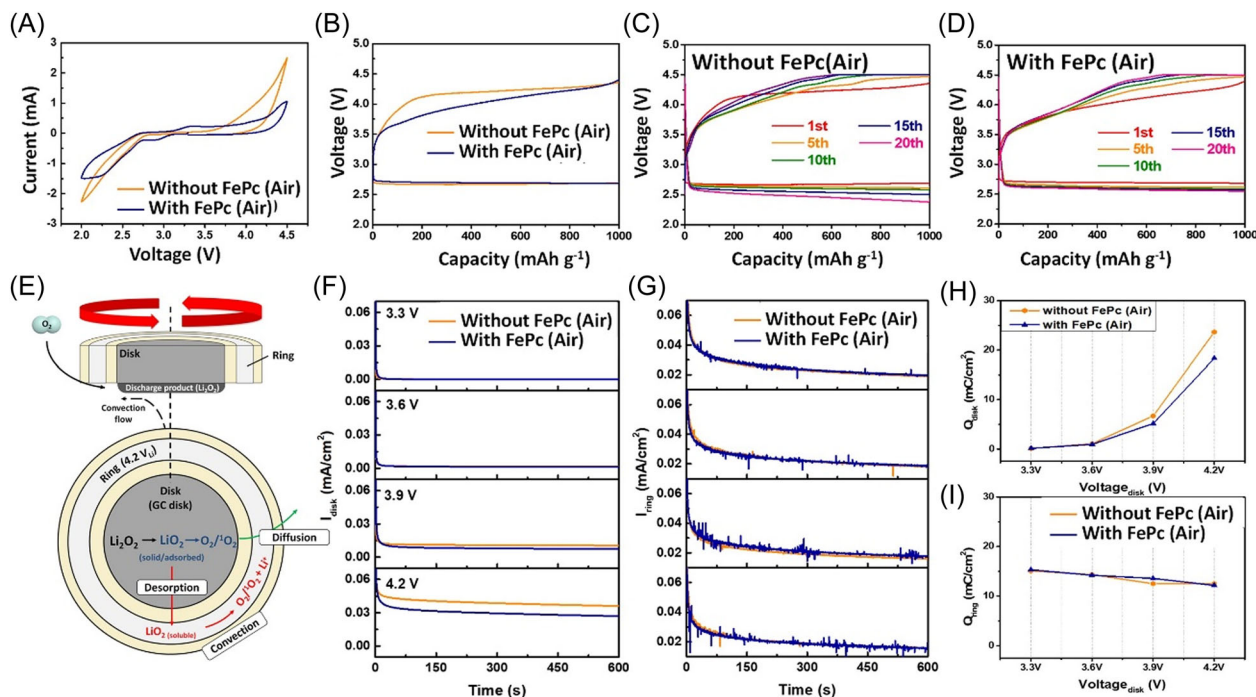


**FIGURE 2** (A) CV curves in Li–Air cells with and without FePc in LiTFSI + TEGDME solutions. (B) Discharge–charge curves with and without FePc in LiTFSI + TEGDME solutions in air atmosphere. Cycling performance of Li–Air cells (C) without FePc and (D) FePc-containing electrolyte in the 4.5–2.3 V voltage window under the specific capacity limit of 1000 mA h g<sup>-1</sup> at a current density of 100 mA g<sup>-1</sup>. (E) Schematic diagram of RRDE for Li<sub>2</sub>O<sub>2</sub> oxidation. Chronoamperometric transients for Li<sub>2</sub>O<sub>2</sub> oxidation on the disk electrode in 0.2 M LiTFSI/TEGDME and FePc-containing 0.2 M LiTFSI/TEGDME electrolyte in Li–Air battery. (F) Disk current transients. (G) Ring current transients. (H) The capacity on the disk at a corresponding potential. (I) The capacity on the ring at a corresponding potential. The Au ring was held at 4.0 V<sub>Li</sub>.

4.2 V is sufficient to fully decompose the discharge products.

Figure 2F,G shows the current values for the disk and ring measured at each disk potential in the air atmosphere. Based on the chronoamperometric transient current curves in Figure 2F,G, the amounts of electric charge are calculated by integrating the graphs as shown in Figure 2H,I for each voltage. The maximum disk currents in Figure 2F are obtained at the initial state of each potential, after which they degrade to small stable values, indicating a diffusion-dominant process (e.g., diffusion of Li<sup>+</sup> in solid Li<sub>2</sub>O<sub>2</sub>).<sup>32</sup> The charge currents of the disk electrode gradually increase by increasing the applied voltage from 3.3 to 4.2 V<sub>Li</sub>. At 4.2 V<sub>Li</sub>, the amount of charge (Q) in the Li–Air battery increases rapidly in both the pristine and FePc-containing cells, which occurs due to the decomposition of the discharge products (Li<sub>2</sub>CO<sub>3</sub>, Li<sub>2</sub>O<sub>2</sub>, and Li<sub>2</sub>O) and the inevitable electrolyte decomposition at high voltage (Figure 2H).<sup>33</sup> It is well known that superoxide ions (O<sub>2</sub><sup>-</sup>) are produced during the charge/discharge process of a Li–Air battery. These oxides are very reactive and go through side reactions with the electrolyte and electrode surface.<sup>34</sup> In the case of cells using FePc, however, we observe a lower amount of charge (Q)

because FePc stabilizes the reactive oxygen radicals and simultaneously prevents unwanted side reactions. It can also be seen that FePc stabilizes O<sub>2</sub><sup>-</sup> in the Li–O<sub>2</sub> cell (Figure S1). The results confirm that the disk and ring currents of the FePc-containing cell are lower at 4.2 V than those of the pristine cell in a pure O<sub>2</sub> atmosphere (Figure S1a,b), indicating that FePc stabilizes the O<sub>2</sub><sup>-</sup>. In addition, the amounts of charge in the FePc-containing cell are 2.22 and 2.87 mC cm<sup>-2</sup> in the disk and ring, respectively, which are lower than that in the pristine cell (2.72 mC<sub>disk</sub> cm<sup>-2</sup> and 3.17 mC<sub>ring</sub> cm<sup>-2</sup>, respectively) (Figure S1c). The amount of charge in the ring electrode (Q<sub>ring</sub>) is relatively high (3.9 V<sub>Li</sub>), especially in FePc-containing cells (Figure 2I). This is because FePc promotes the transfer of CO<sub>2</sub> and O<sub>2</sub> in the ambient air, thereby improving the formation of lithium carbonate (Li<sub>2</sub>CO<sub>3</sub>) and lithium peroxide (Li<sub>2</sub>O<sub>2</sub>) during discharge.

## 2.2 | Identification of the products and reversible Li–O<sub>2</sub>/Li–Air reaction

To further examine the reversibility and surface reaction characteristics of LOB and LAB, we conducted diverse ex

situ surface and structural analyses of the electrodes (pristine, after discharge, and after charge) in O<sub>2</sub> and air atmospheres. The X-ray diffraction (XRD) patterns in Figure 3A show the crystalline structure of electrodes collected at different electrochemical charging states and purging conditions. There is no dominant XRD peak associated with Li<sub>2</sub>O<sub>2</sub> or Li<sub>2</sub>CO<sub>3</sub> for any of the samples in the LOB, suggesting that the discharge products under the O<sub>2</sub> atmosphere are formed in an amorphous phase.<sup>14,29,35</sup> By contrast, the peaks related to Li<sub>2</sub>CO<sub>3</sub> in the LAB are clearly visible after the electrode discharge, indicating that crystalline Li<sub>2</sub>CO<sub>3</sub> products form in the air atmosphere. The discharge product containing Li<sub>2</sub>CO<sub>3</sub> is confirmed to reversibly decompose after the charge process, as evidenced by the absence of Li<sub>2</sub>CO<sub>3</sub> peaks. Because the oxide products are amorphous, the discharge products would exist as co-phases of oxide and carbonate. The ex situ Raman spectra (Figure 3B) show a peak related to the O–O stretching frequency in LiO<sub>2</sub>, which appears around 1125 cm<sup>-1</sup> after the electrode discharge in both O<sub>2</sub> and air atmospheres and disappears reversibly after charge.<sup>36</sup> To further examine the chemical structure of the discharge products, we conducted

Fourier transform infrared spectroscopy (FT-IR) for the electrodes operated in O<sub>2</sub> and air atmospheres (Figure 3C). Peaks related to Li<sub>2</sub>CO<sub>3</sub> appear at 1420 cm<sup>-1</sup> after discharge and disappear after recharging for both O<sub>2</sub> and air purging. The surface morphologies of the samples after cycling were analyzed using scanning electron microscopy (SEM) for the pristine, discharged, and charged electrodes (Figure S2). During discharge, the Ni foam substrate is covered with the discharge products in both O<sub>2</sub> and air atmospheres. After the charging process, the discharge products reversibly decompose. The result is consistent with the previous ex situ results, suggesting that FePc exhibits catalytic activities in LAB even in a 20 vol% O<sub>2</sub> atmosphere.

To examine the changes in chemical bonding occurring in different electrochemical charging states, we performed ex situ X-ray photoelectron spectroscopy (XPS) for the LOB and LAB (Figures 4A–D and S3). The C 1s spectra of the pristine, discharged, and charged electrodes show common peaks corresponding to the C–C and C–O bonds in both O<sub>2</sub> and air atmospheres (Figure 4A,B). In the LOB, the intensities of the peaks related to the C–C bond in all electrodes are similar to

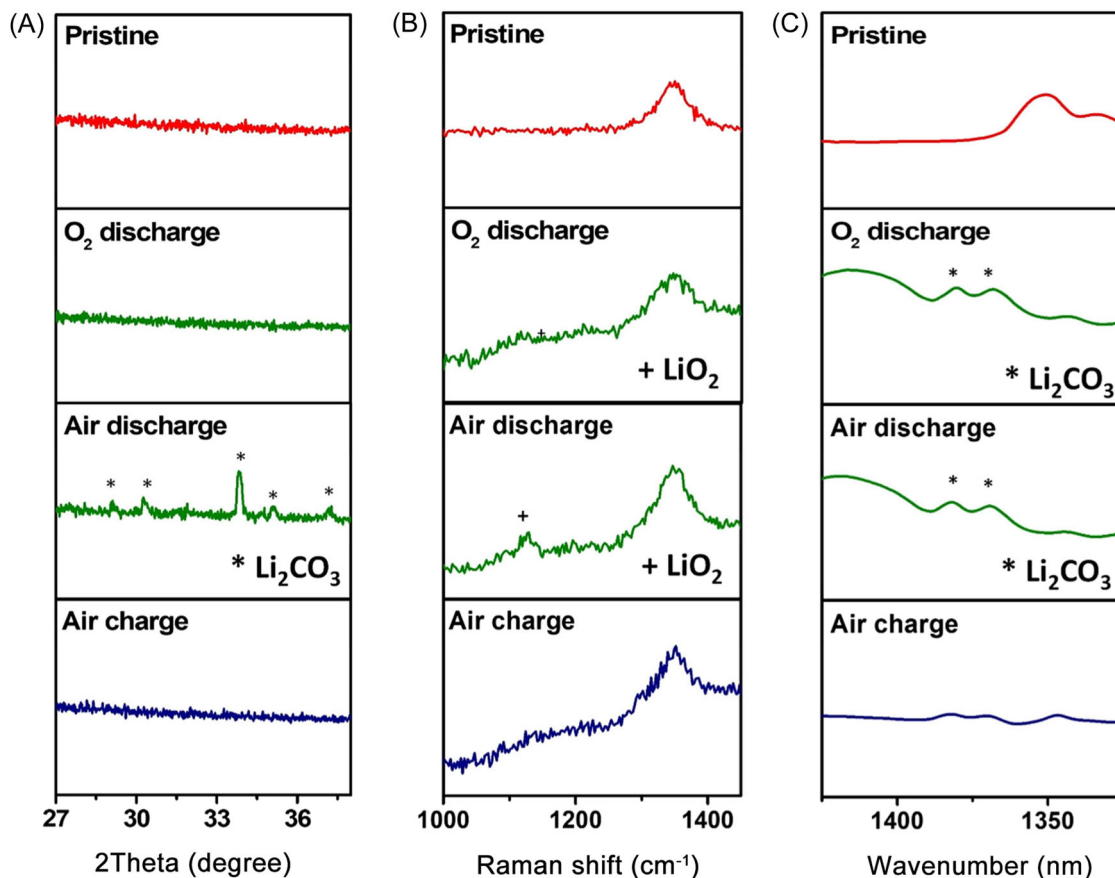
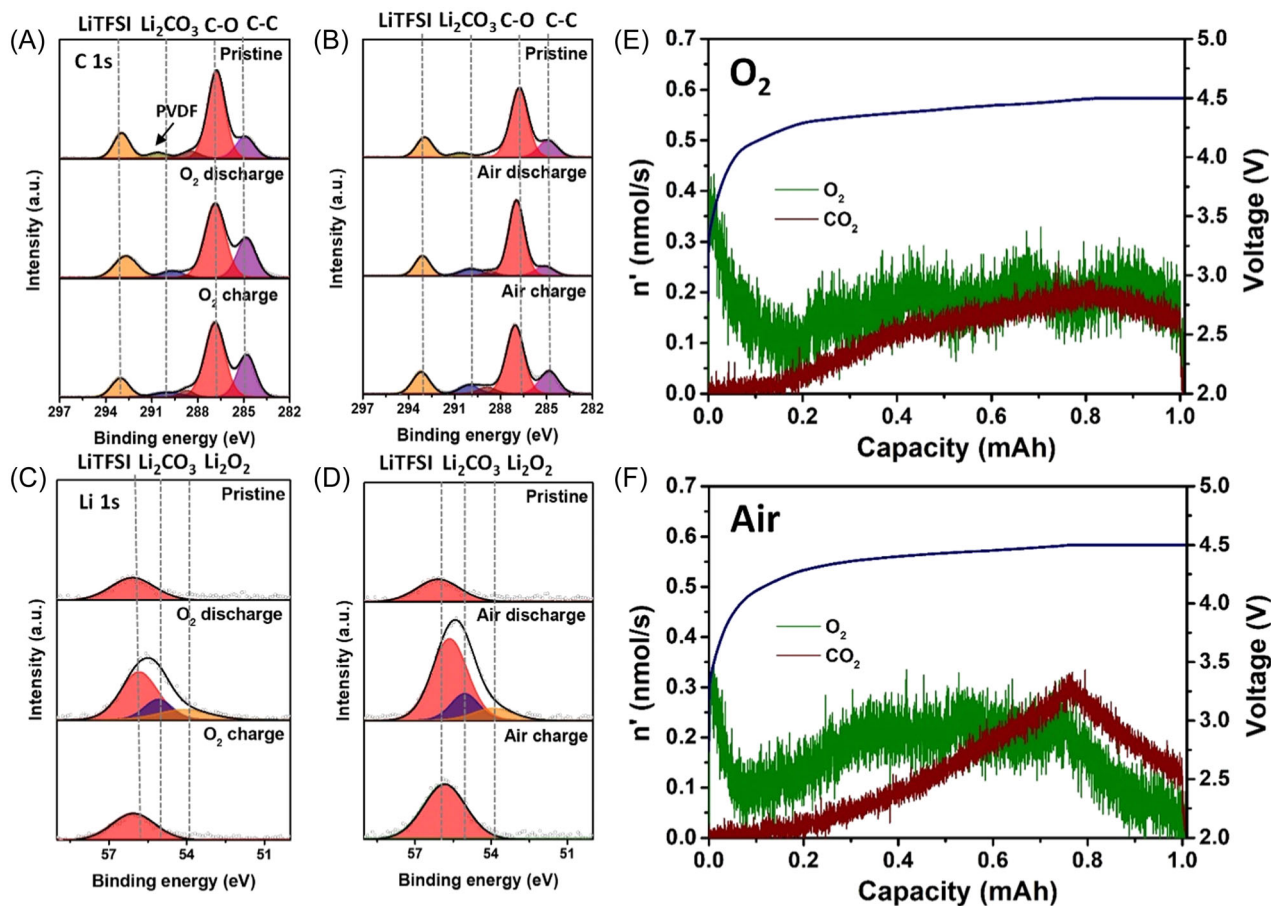


FIGURE 3 (A) XRD patterns, (B) Raman spectra, and (C) FT-IR results obtained for pristine, discharged, and charged electrodes in Li–O<sub>2</sub> and Li–Air cells.



**FIGURE 4** Ex situ XPS spectra obtained for the electrode after each stage, collected in the (A) C 1s and (B) C 1s for Li–O<sub>2</sub> battery and (C) Li 1s, (D) Li 1s for Li–Air battery. In situ DEMS results show the O<sub>2</sub> and CO<sub>2</sub> gas evolution rates during charging in (E) Li–O<sub>2</sub> and (F) Li–Air cells.

each other. However, the C–C peak in the LAB seems to have decreased significantly. These results indicate that the discharge products of both Li<sub>2</sub>O<sub>2</sub> and Li<sub>2</sub>CO<sub>3</sub> cover the electrode surface after charge/discharge in the air atmosphere. Likewise, the peak representing the poly(vinylidene fluoride) (PVdF) binder also weakens after discharge, and the carbon electrode surface is covered by the discharge products. Furthermore, a weak peak at 289.6 eV corresponding to Li<sub>2</sub>CO<sub>3</sub> is also detected after discharge and then decreases in intensity after charge, which implies the reversible decomposition of the discharge products in the FePc-containing LOB and LAB. The Li 1s spectra show a peak associated with bis(trifluoromethane)sulfonimide lithium salt (LiTFSI) salt (56 eV) for all the electrodes (Figure 4C,D). The peaks corresponding to the discharge products, such as Li<sub>2</sub>O<sub>2</sub> and Li<sub>2</sub>CO<sub>3</sub>, appear after discharge and completely disappear after charge. Similarly, a peak related to Li<sub>2</sub>O<sub>2</sub> appears in the O 1s spectra after discharge and then completely disappears during the charging process (Figure S3). The reversibility of the discharge/charge

reactions is also confirmed by the peaks related to the LiTFSI salt in the electrolyte. The LiTFSI peak is observed at 398.8 eV in the N 1s spectra of all three samples. In the discharged sample, however, a new peak appears around 397.4 eV as the LiTFSI peak decreases, which implies the formation of Li<sub>3</sub>N by reduction of LiTFSI during discharge.<sup>37</sup> Interestingly, the peak on Li<sub>3</sub>N reversibly disappears after charge, indicating improved reversibility by FePc catalysis in LABs. In addition, we confirmed the reversible decomposition of the discharge products by analyzing the gas evolution using in situ DEMS tests (Figure 4E,F). In the initial stage of charge, O<sub>2</sub> evolution prevails as Li<sub>2</sub>O<sub>2</sub> decomposes into Li<sup>+</sup> ions and O<sub>2</sub> (Li<sub>2</sub>O<sub>2</sub> → Li<sup>+</sup> + O<sub>2</sub> + 2e<sup>-</sup>) in both O<sub>2</sub> and air atmospheres. Moreover, CO<sub>2</sub> evolution gradually increases along with O<sub>2</sub> as the reaction proceeds, which is attributed to the decomposition of Li<sub>2</sub>CO<sub>3</sub> formed during the discharging process. In particular, the results confirm that a larger amount of CO<sub>2</sub> is generated in the air atmosphere than that in the O<sub>2</sub> atmosphere, which is due to the smoother decomposition

of  $\text{Li}_2\text{CO}_3$ , which functions as an insulating by-product during the charging process of the FePc-containing LAB (Figure 4F). These results indicate remarkable catalytic properties of FePc, which enable outstanding electrochemical performances of not only the LOB but also the  $\text{CO}_2$ -containing LAB.

### 2.3 | Reaction pathway and catalytic effects of FePc-containing Li-O<sub>2</sub>/Li-Air cells

To clarify the manner of FePc's participation in the actual reaction process, it is necessary to monitor the chemical and structural variation of FePc in real time during the reaction. Therefore, we conducted in situ spectroelectrochemical analyses to confirm the changes in FePc during the reactions (Figure 5). In Figure 5A, the in situ UV-vis spectra of FePc were acquired between 200 nm and 800 nm during CV scanning in a 1.0 M LiTFSI + tetraethylene glycol dimethyl ether (TEGDME) solution under an  $\text{O}_2$  atmosphere. Generally, the UV-vis spectrum for MPcs exhibits two bands: (1) the B-band in the range 200–400 nm, attributed to the  $\pi$ - $\pi^*$  electron transitions, and (2) the Q-band in the range 500–800 nm,

attributed to the  $n$ - $\pi^*$  electron transitions between the bonding and anti-bonding molecular orbitals.<sup>38</sup> Based on these transitions, the characteristic FePc spectra (especially the Q-band) start to appear around 650 nm at a voltage of 3.3 V. As the voltage decreases during discharge, the intensity of the main peak around 650 nm decreases, and a new peak forms around 600 nm. As can be seen from Figure S4, this blue-shifting peak appears as electrons move from the metal to the ligand as  $\text{O}_2$  binds to the central metal of Fe and is referred to as the “charge transfer band.”<sup>39–43</sup> As the charge process recurs (voltage increases from 2.0 to 4.0 V), the intensity of this charge transfer band decreases, and the intensity of the main peak increases reversibly. The shift in the FePc peak and subsequent reversion to the original range mean that the FePc-mediated catalytic reaction is reversible. This is seen more clearly in Figure 5B, where the three-dimensional profile is converted to a two-dimensional contour plot. In the corresponding graph, red means the peak part with the largest absorbance of UV-vis, and as it goes blue, the intensity of absorbance becomes less. Similarly, the main FePc peak appears around 650 nm, blue-shifts to 600 nm as discharging is performed, and subsequently returns to the original position of the main peak during charge.

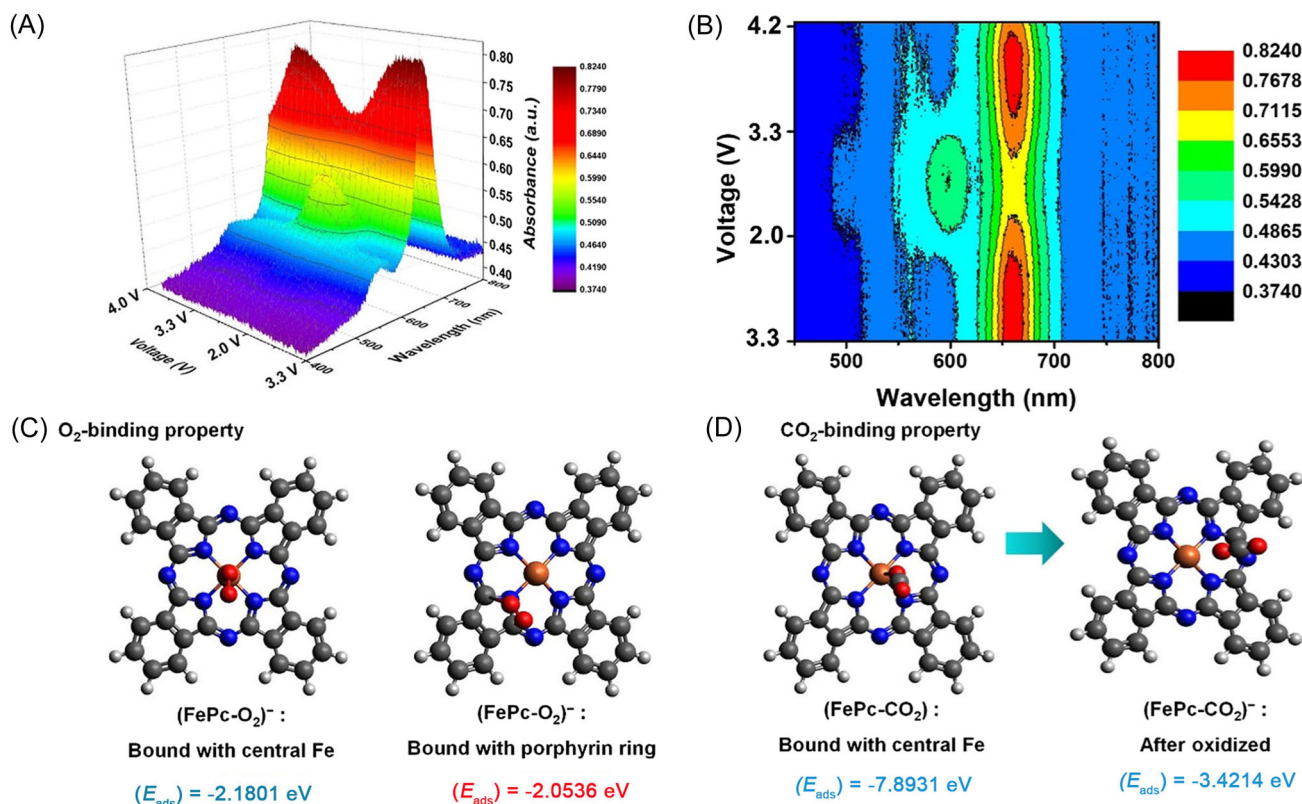
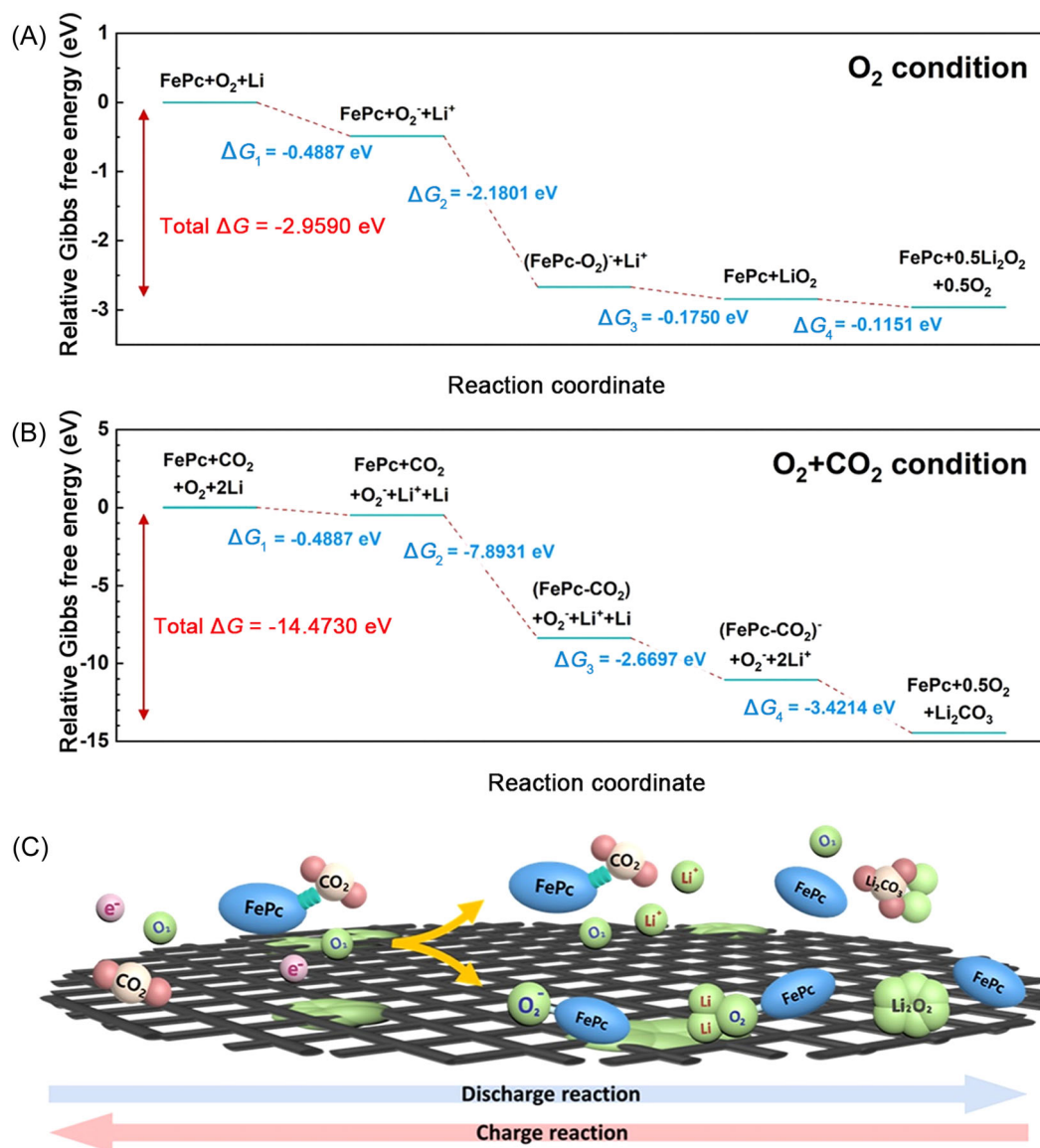


FIGURE 5 Spectroelectrochemical results of 1.0 M LiTFSI + TEGDME + FePc. (A) UV-vis spectrum of 1.0 M LiTFSI + TEGDME + FePc. (B) Contour plot showing the absorbance changes of Fe ion during the cycling. (C) Predicted molecular structures of  $(\text{FePc-O}_2)^-$ . (D) Predicted molecular structures of  $\text{FePc-CO}_2$  and  $(\text{FePc-CO}_2)^-$ .



**FIGURE 6** Relative Gibbs free energy diagrams for FePc in (A) O<sub>2</sub> condition and (B) O<sub>2</sub> + CO<sub>2</sub> condition. (C) Schematic illustration for reaction mechanisms in Li-Air cells fabricated using FePc.

In addition, the detailed binding properties of FePc were predicted using first-principles calculations. In the case of O<sub>2</sub> binding, the pristine FePc spontaneously captures the oxygen radical through the central Fe ion, exhibiting an adsorption energy (ΔG) of -2.18 eV (Figure 5C). The adsorption energy of the porphyrin ring is lower (-2.05 eV), indicating that it is not energetically favorable. A similar reaction occurs in the case of CO<sub>2</sub> binding, as shown in Figure 5D. Interestingly, FePc spontaneously reacts with CO<sub>2</sub>, lowering the total Gibbs free energy by -7.89 eV, which is a fairly high value than that for O<sub>2</sub> adsorption. In this process, CO<sub>2</sub> adsorption occurs only through the central Fe ion, which is different from O<sub>2</sub> adsorption. Moreover, the oxidized

FePc immediately releases CO<sub>2</sub> while further lowering the Gibbs free energy by -2.67 eV. This result indicates that the unique catalytic reaction of FePc with auto-CO<sub>2</sub>-binding properties enables its practical implementation as an RM in an air atmosphere.

Next, we performed first-principles calculations to predict the catalytic effects of FePc on the reaction pathways during charge/discharge in LABs. Figure 6 depicts the changes in total Gibbs free energy of each intermediate under O<sub>2</sub> and O<sub>2</sub> + CO<sub>2</sub> atmospheres. The changes show a continuous decrease in the total Gibbs free energy in both atmospheres, implying that FePc functions well as an RM in LABs. In the O<sub>2</sub> atmosphere, FePc binds spontaneously with highly reactive oxygen

radicals ( $\cdot\text{O}_2^-$ ) during the ORR process (Figure 6A). In this reaction, the Gibbs free energy is reduced by  $-2.18$  eV, indicating that oxygen radicals can be effectively captured and stabilized by the high adsorption energy of FePc. Then, they successively react with neighboring  $\text{Li}^+$  to form lithium oxides ( $\text{LiO}_2$  and  $\text{Li}_2\text{O}_2$ ), which is consistent with the results reported in a previous study.<sup>34</sup> However, the results predict that the reaction pathway of FePc-containing LABs is significantly changed in an  $\text{O}_2 + \text{CO}_2$  atmosphere. As shown in Figure 6B, FePc first reacts with the  $\text{CO}_2$  molecule and withdraws electrons from a nearby Li to form the  $\text{Li}^+$  ion. During this process, the Gibbs free energy is reduced by  $-7.9$  eV. This indicates that FePc preferentially attracts  $\text{CO}_2$  molecules with high priority. Subsequently, this intermediate reacts with nearby  $\text{Li}^+$  ions and oxygen radicals ( $\cdot\text{O}_2^-$ ) to form lithium oxides. Considering the diversity of the obtained carbon-based products, the formation of only  $\text{Li}_2\text{CO}_3$  should be thermodynamically favorable. In alternative catalytic reaction pathways, the formation of additional carbon and carbon monoxide (CO) species is accompanied by an increase in the Gibbs free energy; thus, the formation of these reactants is thermodynamically unsuitable (Figure S5). Interestingly, the total Gibbs free energy in the  $\text{O}_2 + \text{CO}_2$  atmosphere is reduced by  $-14.47$  eV, which is considerably larger than the changes in Gibbs free energy in the  $\text{O}_2$  atmosphere ( $-2.959$  eV). The results of the first-principles calculations imply that the FePc-containing LAB can initially react with  $\text{CO}_2$  rather than  $\text{O}_2$ , even in an  $\text{O}_2$  atmosphere containing very small amounts of  $\text{CO}_2$  (similar to the air atmosphere). Therefore, the results confirm that FePc effectively exhibits a catalytic effect in the air atmosphere, which improves the electrochemical performance of LAB. In addition, the Gibbs free energy results show that  $\text{O}_2$  and  $\text{CO}_2$  bind competitively to the central metal of FePc in the air atmosphere (Figure 6C).

### 3 | CONCLUSION

In summary, by introducing FePc to Li–Air batteries, we were able to confirm two properties of FePc: (1) the reduction in overpotential and improvement in cell performance and (2) the suppression of side reactions (electrolyte decomposition) in the high voltage range. Through RRDE analysis, we demonstrated that using FePc simultaneously promotes the battery reaction and suppresses the electrolyte decomposition in the high voltage range (over 4.0 V). This phenomenon occurs when FePc binds with highly reactive superoxide radical ions to suppress side reactions. The reversible formation and decomposition of the discharge products were confirmed through ex situ XRD, FT-IR, Raman and

XPS analyses, and in situ DEMS characterization of the cells. To gain insight into the reaction mechanism and improvement in performance for the LAB using FePc as a catalyst for electrolytes, possible intermediates and pathways were investigated by theoretical predictions, which showed that when FePc is used in an air atmosphere,  $\text{O}_2$  and  $\text{CO}_2$  competitively bind with the central metal of FePc and proceed with the reaction. In particular, despite being present in small amounts,  $\text{CO}_2$  was observed to bind with FePc faster than  $\text{O}_2$ .

## 4 | EXPERIMENTAL SECTION

### 4.1 | Materials and chemicals

FePc, LiTFSI (99.95%), TEGDME (99%), PVdF (Mw  $\sim 180,000$ ), 1-methyl-2-pyrrolidinon (NMP, anhydrous, 99.5%), and potassium dioxide were purchased from Sigma-Aldrich (Korea). The moisture was removed from TEGDME by dipping freshly activated molecular sieves (type 4 Å) in the solvent for 2 weeks.

### 4.2 | Preparation of Li– $\text{O}_2$ /Li–Air cells

The oxygen/air ( $\text{O}_2$ /Air) electrode was fabricated by preparing a slurry containing 90 wt% multiwalled carbon nanotubes (MWCNT) and 10 wt% PVdF dissolved in NMP solution. The slurry was coated onto an Ni foam (12 mm in diameter) used as the current collector and dried under vacuum at  $80^\circ\text{C}$  overnight. The average mass loading of the slurry was 0.4 mg per 12-mm diameter of the Ni foam. The pristine electrolyte was fabricated with 1.0 M LiTFSI in TEGDME stirred for 24 h at room temperature. To prepare the FePc-RMs, 0.1 g of phthalocyanine molecules and 1.0 M LiTFSI were dissolved in 0.5 ml TEGDME and stirred for 24 h in an Ar-filled glove box to saturate the precursor solution. The supernatant of the FePc-RM saturated solution was used as the electrolyte. A 12-mm-diameter Li–metal foil was used as the anode, and a glass fiber (Whatman GF/A microfiber filter paper) was used as the separator. Coin cells containing multiple holes were used for the CV, full discharge/charge, and cycling tests. All the cells were assembled in an Ar-filled glove box. The cells were purged with  $\text{O}_2$  (99.999%) and air ( $\text{O}_2$  21%,  $\text{N}_2$  79%), respectively, before the tests.

### 4.3 | Electrochemical characterization

The catalytic effect of FePc-containing cells was analyzed via CV (a Biologic VSP potentiostat with impedance

function) in the voltage range 2.0–4.5 V and increasing scan rates up to 5 mV s<sup>-1</sup>. The charge/discharge tests were performed using a potentiogalvanostat (WonATech; WBCS3000) at a current density of 100 mA g<sup>-1</sup> in the voltage range 2.3–4.5 V versus Li<sup>+</sup>/Li. A potentiogalvanostat (WonATech; WBCS3000L) was used for the cycling tests that were performed at a current density of 100 mA g<sup>-1</sup> with a limited capacity of 1000 mAh g<sup>-1</sup> in the same voltage range as the charge/discharge tests. The cells were purged with O<sub>2</sub>/Air gas before all electrochemical tests, and the tests were performed at room temperature.

#### 4.4 | Material characterization

XPS (K-alpha; Thermo Fisher Scientific UK) was performed for material characterization and surface analysis. A field emission SEM was used to image the MWCNT-loaded electrodes. A UV-vis spectrophotometer was used to investigate the oxygen-binding effect of phthalocyanine.

#### 4.5 | In situ spectroelectrochemical measurement

The spectroelectrochemical measurement was carried out to monitor the chemical changes of the FePc molecule during discharge and charge. The electrolytes were transferred into a quartz cuvette with a commercial Au honeycomb electrode (Pine Research Instrumentation). The working electrode was perforated with a honeycomb pattern of holes that allowed light to pass through the electrode. The active surface of the working electrode had an Au coating along the inner walls of the holes. As the light beam from the spectrometer passes through the holes, the beam grazes the walls of each hole. A Pt counter electrode and a Pt pseudoreference electrode were used to construct the three-electrode cell. The electrode potential was controlled with a potentiostat (between -0.97 and 1.23 V vs. standard hydrogen electrode), and UV-vis spectra were collected at varying potentials via a Varian Cary 50 spectrophotometer. The electrolytes were purged with dry O<sub>2</sub>/Air for a minimum of 20 min before each experiment. All the potential values for CVs were calibrated against voltage versus Li<sup>+</sup>/Li ( $E^0 = -3.04$  V).

#### 4.6 | Ex situ characterizations

The surface characterization of the electrodes after cycling was investigated by XPS measurements.

The surface morphologies after cycling were observed using SEM imaging. The samples were prepared by galvanostatic discharging and charging at a current density of 100 mA g<sup>-1</sup>, and each electrode was collected after the first discharging and charging cycle with no capacity limit. A pristine electrode dipped in the electrolyte was prepared for comparison. The cells were disassembled in an Ar-filled glove box after discharging and charging, similar to the pristine electrode.

#### 4.7 | RRDE

The RRDE cell was composed of a Pt counter electrode (diameter 0.5 mm, length 23 cm; ALS Co., Ltd.), a nonaqueous reference electrode (Ag/Ag<sup>+</sup>) (ALS Co., Ltd.) calibrated against Li metal ( $0 V_{Li} \approx -3.27 \pm 0.03$  V vs. Ag/Ag<sup>+</sup> for TEGDME), an RRDE, and an electrolyte (0.2 M LiTFSI/TEGDME). The working electrode consisted of a GC disk of 4.0 mm in diameter surrounded by an Au ring with an internal diameter of 5 mm and an external diameter of 7 mm (ALS Co., Ltd.).

#### 4.8 | Computational details

The geometry optimization and energy evaluation of the RM molecules were conducted using a Gaussian 16 package.<sup>44</sup> For all the calculations, spin-unrestricted density functional theory was performed based on the Becke-Lee-Yang-Parr hybrid exchange-correlation functional<sup>45-47</sup> and triple-zeta valence polarization basis set.<sup>47-49</sup> The molecular structure of calculated FePc was visualized using Avogadro software.<sup>50</sup> The effect of TEGDME solvation was considered by applying a dielectric constant of 7.9, as used in previous studies.<sup>34,51,52</sup>

#### AUTHOR CONTRIBUTIONS

Boran Kim and Won-Hee Ryu designed the research and performed the experimental data analysis. Boran Kim and Hyun-Soo Kim conducted the electrochemical experiments and surface analysis for the electrodes and collected the data. Boran Kim and Jun Seo Lee conducted the electrochemical chronoamperometry experiments through RRDE analysis. Hyunyoung Park and Jongsoo Kim contributed to the first-principles calculations. All authors co-wrote the manuscript. Won-Hee Ryu supervised the work. All authors discussed the results and commented on the manuscript.

#### ACKNOWLEDGMENTS

This study was supported by the National Research Foundation of Korea (NRF) grant funded by the Korean

government (MSIT) (Nos. 2022M3J1A1085410 and RS-2023-00208983).

## CONFLICT OF INTEREST STATEMENT

The authors declare that there are no conflicts of interests.

## ORCID

Jongsoon Kim  <http://orcid.org/0000-0002-7651-5516>

Won-Hee Ryu  <http://orcid.org/0000-0002-0203-2992>

## REFERENCES

- Lee J-Y, Kim H-S, Lee J-S, Park C-J, Ryu W-H. Blood protein as a sustainable bifunctional catalyst for reversible Li-CO<sub>2</sub> batteries. *ACS Sustainable Chem Eng*. 2019;7(19):16151-16159.
- Kim H-S, Lee J-Y, Yoo J-K, Ryu W-H. Capillary-driven formation of iron nanoparticles embedded in nanotubes for catalyzed lithium-carbon dioxide reaction. *ACS Mater Lett*. 2021;3(6):815-825.
- Thackeray MM, Wolverton C, Isaacs ED. Electrical energy storage for transportation—approaching the limits of, and going beyond, lithium-ion batteries. *Energy Environ Sci*. 2012;5(7):7854-7863.
- Huang G, Wang J, Zhang X. Electrode protection in high-efficiency Li-O<sub>2</sub> batteries. *ACS Cent Sci*. 2020;6(12):2136-2148.
- Zhang T, Zhou H. From Li-O<sub>2</sub> to Li-air batteries: carbon nanotubes/ionic liquid gels with a tricontinuous passage of electrons, ions, and oxygen. *Angew Chem Int Ed*. 2012;51(44):11062-11067.
- Ryu W-H, Yoon T-H, Song SH, Jeon S, Park YJ, Kim ID. Bifunctional composite catalysts using Co<sub>3</sub>O<sub>4</sub> nanofibers immobilized on nonoxidized graphene nanoflakes for high-capacity and long-cycle Li-O<sub>2</sub> batteries. *Nano Lett*. 2013;13(9):4190-4197.
- Girishkumar G, McCloskey B, Luntz AC, Swanson S, Wilcke W. Lithium-air battery: promise and challenges. *J Phys Chem Lett*. 2010;1(14):2193-2203.
- Padbury R, Zhang X. Lithium-oxygen batteries—limiting factors that affect performance. *J Power Sources*. 2011;196(10):4436-4444.
- Mei J, Liao T, Liang J, Qiao Y, Dou SX, Sun Z. Toward promising cathode catalysts for nonlithium metal-oxygen batteries. *Adv Energy Mater*. 2020;10(11):1901997.
- Mei J, Wang J, Gu H, et al. Nano polymorphism-enabled redox electrodes for rechargeable batteries. *Adv Mater*. 2021;33(8):2004920.
- Song L-N, Zhang W, Wang Y, et al. Tuning lithium-peroxide formation and decomposition routes with single-atom catalysts for lithium-oxygen batteries. *Nat Commun*. 2020;11(1):2191.
- Lim HD, Song H, Kim J, et al. Superior rechargeability and efficiency of lithium-oxygen batteries: hierarchical air electrode architecture combined with a soluble catalyst. *Angew Chem*. 2014;126(15):4007-4012.
- Black R, Lee JH, Adams B, Mims CA, Nazar LF. The role of catalysts and peroxide oxidation in lithium-oxygen batteries. *Angew Chem Int Ed*. 2013;52(1):392-396.
- Lee J-S, Lee C, Lee J-Y, Ryu J, Ryu W-H. Polyoxometalate as a nature-inspired bifunctional catalyst for lithium-oxygen batteries. *ACS Catal*. 2018;8(8):7213-7221.
- Lee J-S, Kim H-S, Ryu W-H. Iron/carbon composite microfiber catalyst derived from hemoglobin blood protein for lithium-oxygen batteries. *Appl Surf Sci*. 2019;466(4):562-567.
- Gao X, Chen Y, Johnson LR, Jovanov ZP, Bruce PG. A rechargeable lithium-oxygen battery with dual mediators stabilizing the carbon cathode. *Nat Energy*. 2017;2(9):17118.
- Kwak W-J, Mahammed A, Kim H, et al. Controllable and stable organometallic redox mediators for lithium oxygen batteries. *Mater Horiz*. 2020;7(1):214-222.
- Yao KPC, Frith JT, Sayed SY, et al. Utilization of cobalt bis(terpyridine) metal complex as soluble redox mediator in Li-O<sub>2</sub> batteries. *J Phys Chem C*. 2016;120(30):16290-16297.
- Matsuda S, Mori S, Kubo Y, Uosaki K, Hashimoto K, Nakanishi S. Cobalt phthalocyanine analogs as soluble catalysts that improve the charging performance of Li-O<sub>2</sub> batteries. *Chem Phys Lett*. 2015;620(3):78-81.
- Matsuda S, Mori S, Hashimoto K, Nakanishi S. Transition metal complexes with macrocyclic ligands serve as efficient electrocatalysts for aprotic oxygen evolution on Li<sub>2</sub>O<sub>2</sub>. *J Phys Chem C*. 2014;118(49):28435-28439.
- Sun D, Shen Y, Zhang W, et al. A solution-phase bifunctional catalyst for lithium-oxygen batteries. *J Am Chem Soc*. 2014;136(25):8941-8946.
- Abbaspour A, Mirahmadi E. Electrocatalytic activity of iron and nickel phthalocyanines supported on multi-walled carbon nanotubes towards oxygen evolution reaction. *Electrochim Acta*. 2013;105(19):92-98.
- Gunasekara I, Ates MN, Mukerjee S, Plichta EJ, Hendrickson MA, Abraham KM. Solid phase FePC catalysts for increased stability of oxygen reduction reaction intermediates at the cathode/electrolyte interface in lithium air batteries. *J Electrochem Soc*. 2017;164(4):A760-A769.
- Tang C, Zhang Q. Can metal-nitrogen-carbon catalysts satisfy oxygen electrochemistry? *J Mater Chem A*. 2016;4(14):4998-5001.
- Yu L, Shen Y, Huang Y. FeNC catalyst modified graphene sponge as a cathode material for lithium-oxygen battery. *J Alloys Compd*. 2014;595(14):185-191.
- Arul A, Pak H, Moon KU, Christy M, Oh MY, Nahm KS. Metallomacrocyclic-carbon complex: a study of bifunctional electrocatalytic activity for oxygen reduction and oxygen evolution reactions and their lithium-oxygen battery applications. *Appl Catal B*. 2018;220(1):488-496.
- Verma C, Ebenso EE, Quraishi MA, Rhee KY. Phthalocyanine, naphthalocyanine and their derivatives as corrosion inhibitors: a review. *J Mol Liq*. 2021;334(14):116441.
- Ohtsuka M, Kitamura F. On the formal redox potential of oxygen reduction reaction at iron phthalocyanine/graphene composite electrode in alkaline media. *Electrochemistry*. 2015;83(5):376-380.
- Ryu W-H, Gittleson FS, Thomsen JM, et al. Heme biomolecule as redox mediator and oxygen shuttle for efficient charging of lithium-oxygen batteries. *Nat Commun*. 2016;7(1):12925.
- Wang Y, Lu Y-R, Dong C-L, Lu Y-C. Critical factors controlling superoxide reactions in lithium-oxygen batteries. *ACS Energy Lett*. 2020;5(5):1355-1363.
- Tan C, Cao D, Zheng L, Shen Y, Chen L, Chen Y. True reaction sites on discharge in Li-O<sub>2</sub> batteries. *J Am Chem Soc*. 2022;144(2):807-815.

32. Yi-Chun L, Yang S-H. Probing the reaction kinetics of the charge reactions of nonaqueous Li-O<sub>2</sub> batteries. *J Phys Chem Lett.* 2012;4(1):93-99.
33. Kwak W-J, Park J-B, Jung H-G, Sun Y-K. Controversial topics on lithium superoxide in Li-O<sub>2</sub> batteries. *ACS Energy Lett.* 2017;2(12):2756-2760.
34. Kim HS, Kim B, Park H, Kim J, Ryu WH. Auto-oxygenated porphyrin-derived redox mediators for high-performance lithium air-breathing batteries. *Adv Energy Mater.* 2022;12(7):2103527.
35. Yalagala BP, Sankaranarayanan SA, Rengan AK, Vanjari SRK. Biocompatible, flexible, and high-performance nanowelded silver nanowires on silk fibroin for transparent conducting electrodes toward biomemristor application. *ACS Sustainable Chem Eng.* 2022;10(14):4473-4485.
36. Yang J, Zhai D, Wang H-H, et al. Evidence for lithium superoxide-like species in the discharge product of a Li-O<sub>2</sub> battery. *Phys Chem Chem Phys.* 2013;15(11):3764-3771.
37. Nilsson V, Younesi R, Brandell D, Edström K, Johansson P. Critical evaluation of the stability of highly concentrated LiTFSI-acetonitrile electrolytes vs. graphite, lithium metal and LiFePO<sub>4</sub> electrodes. *J Power Sources.* 2018;384(12):334-341.
38. Yang H, Qiao L, Peng X, et al. Structural properties of iron phthalocyanine thin films on solid surfaces by drop casting deposition. *J Mater Sci: Mater Electron.* 2019;30(16):14855-14860.
39. Ardiles P, Trollund E, Isaacs M, Armijo F, Aguirre MJ. Evidence of a stable charge-transfer adduct between 2-mercaptoethanol and cobalt-polytetraaminophthalocyanine. *J Coord Chem.* 2001;54(3-4):183-191.
40. Minor PC, Gouterman M, Lever ABP. Electronic spectra of phthalocyanine radical anions and cations. *Inorg Chem.* 1985;24(12):1894-1900.
41. Nevin WA, Hempstead MR, Liu W, Leznoff CC, Lever ABP. Electrochemistry and spectroelectrochemistry of mononuclear and binuclear cobalt phthalocyanines. *Inorg Chem.* 1987;26(4):570-577.
42. Ortiz B, Park SM, Doddapaneni N. Electrochemical and spectroelectrochemical studies of cobalt phthalocyanine polymers. *J Electrochem Soc.* 1996;143(6):1800-1805.
43. Trollund E, Ardiles P, Aguirre J, Biaggio SR, Rocha-Filho RC. Spectroelectrochemical and electrical characterization of poly (cobalt-tetraaminophthalocyanine)-modified electrodes: electrocatalytic oxidation of hydrazine. *Polyhedron.* 2000; 19(22-23):2303-2312.
44. Frisch M, Trucks G, Schlegel H, et al. *Gaussian 16 Revision C.01.* Gaussian Inc.; 2016.
45. Stephens PJ, Devlin FJ, Chabalowski CF, Frisch MJ. Ab initio calculation of vibrational absorption and circular dichroism spectra using density functional force fields. *J Phys Chem.* 1994;98(45):11623-11627.
46. Lee C, Yang W, Parr RG. Development of the Colle-Salvetti correlation-energy formula into a functional of the electron density. *Phys Rev B.* 1988;37(2):785-789.
47. Becke AD. Density-functional thermochemistry. III. The role of exact exchange. *J Chem Phys.* 1993;98(7):5648-5652.
48. Schäfer A, Horn H, Ahlrichs R. Fully optimized contracted Gaussian basis sets for atoms Li to Kr. *J Chem Phys.* 1992; 97(4):2571-2577.
49. Klaumünzer B, Kröner D, Saalfrank P. (TD-)DFT calculation of vibrational and vibronic spectra of riboflavin in solution. *J Phys Chem B.* 2010;114(33):10826-10834.
50. Hanwell MD, Curtis DE, Lonie DC, Vandermeersch T, Zurek E, Hutchison GR. Avogadro: an advanced semantic chemical editor, visualization, and analysis platform. *J Cheminf.* 2012;4(1):17.
51. Lim H-D, Lee B, Zheng Y, et al. Rational design of redox mediators for advanced Li-O<sub>2</sub> batteries. *Nat Energy.* 2016; 1(6):16066.
52. Lee M, Hong J, Lee B, et al. Multi-electron redox phenazine for ready-to-charge organic batteries. *Green Chem.* 2017; 19(13):2980-2985.

## SUPPORTING INFORMATION

Additional supporting information can be found online in the Supporting Information section at the end of this article.

**How to cite this article:** Kim B, Park H, Kim H-S, Lee JS, Kim J, Ryu W-H. Unraveling reaction discrepancy and electrolyte stabilizing effects of auto-oxygenated porphyrin catalysts in lithium-oxygen and lithium-air cells. *Carbon Energy.* 2024;6:e587. doi:10.1002/cey2.587